Geophysical Prospecting, 2007, **55**, 793–804 doi:10.1111/j.1365-2478.2007.00633.x

Determining the dilation factor in 4D monitoring of compacting reservoirs by rock-physics models

José M. Carcione[1]*, Martin Landrø[2], Anthony F. Gangi[3] and Fabio Cavallini[1]

[1] *Istituto Nazionale di Oceanografia e di Geofisica Sperimentale (OGS), Borgo Grotta Gigante 42c, 34010 Sgonico, Trieste, Italy,*
[2] *Department of Petroleum Engineering and Applied Geophysics, Norges Teknisk-Naturvitenskapelige Universitet (NTNU) and*
[3] *Department of Geology and Geophysics, Texas A&M University, College Station, TX 77843-3114, USA*

Received January 2006, revision accepted January 2007

ABSTRACT

Hydrocarbon depletion and fluid injection cause compaction and stretching of the reservoir and overburden layers. 4D prestack seismic data can be used to detect these changes because compaction/stretching causes changes in traveltimes and seismic velocities. We show that, by using two different petro-elastic models at varying effective pressures, a good approximation is to assume that the fractional changes in layer thickness, $\Delta L/L$, and seismic velocity, $\Delta v/v$, are related by a linear function of $\Delta L/L$. The slope of this function (the dilation factor, $\alpha = (\Delta v/v)/(\Delta L/L)$) is negative and its absolute value generally decreases (shale, low porosity) or increases (sandstone, high porosity) with increasing layer thickness and decreasing effective pressure. The analysis is mainly performed for isotropic deformations. The dilation factor for uniaxial deformations is smaller in absolute value.

The dilation factor, which can be calculated from time-lapse data, can be used to predict reservoir compaction/stretching as a function of depth and surface subsidence.

INTRODUCTION

Compaction due to production of hydrocarbons leads to variations in porosity and permeabilities and, therefore, to changes in production performance. Compaction affects the seismic properties of reservoir and overburden rocks. Guilbot and Smith (2002) developed a method that relates differences in the traveltime of a reflection due to compaction and subsidence of the Ekofisk Field in the North Sea. They observed time-shifts of 12–16 ms from 1989 to 1999, related to compaction values of up to 6 m for the reservoir. In some cases, the overburden rocks, constituted mainly by shales, are stretched because the subsidence at the surface is less than the reservoir compaction. This is the case in the Vallhall Field in the North Sea, where the reservoir depth is 2.5 km (Hatchell, Kawar and Savitski 2005). Røste, Stovas and Landrø (2006) developed a method, based on prestack seismic data, to estimate changes in layer thickness and velocity due to compaction. The main uncertainty of the method is in distinguishing between the two effects. To this purpose, they assumed a linear relationship between the fractional changes in the thickness and the velocity changes. Let us denote the vertical traveltime by T, the layer thickness by L and the P-wave velocity of the layer by v. Then, we have, for $T = L/v$, to first order in ΔL and Δv,

$$\frac{\Delta T}{T} = \frac{1}{T}\Delta\left(\frac{L}{v}\right) \approx \frac{\Delta L}{L} - \frac{\Delta v}{v}. \tag{1}$$

Røste *et al.* (2006) assumed the following linear relationship:

$$\frac{\Delta v}{v} = \alpha\frac{\Delta L}{L}, \tag{2}$$

where $\alpha < 0$ is the dilation factor (denoted as R by Hatchell and Bourne (2005a)); i.e. they assumed α to be a constant quantity.

*E-mail: jcarcione@ogs.trieste.it

For an isotropic rock, the volume porosity ϕ is related to the linear porosity ϕ_L by

$$\phi = 1 - (1 - \phi_L)^3 \approx 3\phi_L \tag{3}$$

for $\phi_L \ll 1$, which is valid for three intersecting, mutually perpendicular, planar cracks. For $\phi_L \ll 1$ and an empirical linear relationship between velocity and volume porosity, namely $v = a - b\,\phi$, where a and b are regression parameters, we obtain $\alpha \approx 3b\,(\phi - 1)/v$, because the following relationships hold: $L/L' = (1 - \phi'_L)/(1 - \phi_L)$, $\Delta v/v = (v' - v)/v$ and $\Delta L/L = (\phi'_L - \phi_L)/(1 - \phi'_L)$, which are valid for isotropic expansion or compaction (see equations (17) and (18)), where the prime indicates the post-deformation properties. It can be shown that, for uniaxial expansion or compaction, we have $\alpha \approx b\,(\phi - 1)/v$. Because the velocity variations are more significant than the porosity variations, we may infer that α is approximately inversely proportional to the time-lapse seismic velocity, i.e.

$$\alpha \propto \frac{1}{v}. \tag{4}$$

[Note that this dependence and equation (2) come directly from the following analysis: We may write, for a limited range of effective pressures about P_0, $v = v_0 + \beta_v(P - P_0)$ and $L = L_0 + \beta_L(P - P_0)$. Solving the second equation for $P - P_0$ and substituting it into the first equation gives equation (2) where $\alpha = (\beta_v/\beta_L)(L/v)$, with $\beta_v > 0$ and $\beta_L < 0$.]

Combining equations (1) and (2), we obtain the thickness change as a function of the relative change in traveltime:

$$\frac{\Delta L}{L} = \left(\frac{1}{1-\alpha}\right)\frac{\Delta T}{T}. \tag{5}$$

The purpose of this work is to estimate the dilation factor α from rock-physics models. The expression of the dilation factor in terms of the rock and fluid properties allows us to obtain the velocity and thickness changes in the reservoir and overburden rocks in terms of the observed time-lapse variations in traveltime. Hatchell and Bourne (2005a,b) also used time-lapse time shifts to investigate reservoir compaction. The advantage of using petro-elastic models, apart from the added physical insight, is the possibility of an accurate calibration with laboratory (core data) and well-log data at the microstructural level.

We consider two models: the asperity-deformation model developed by Gangi (1978, 1981) and Gangi and Carlson (1996), and the Hertz–Mindlin model due to Hertz (1895) and later modified by Mindlin (1949), which was further modified by Gangi (1978, 1981). The first model describes cracked media and foliated media with various degrees of contact. The second model is based on a random packing of spherical grains. Both models allow us to obtain the seismic properties as a function of the effective pressure (the differential pressure in the Hertz–Mindlin model).

THEORY

We consider the asperity-deformation and the Hertz–Mindlin models in order to relate changes in layer (rock) thickness to changes in wave velocity.

The asperity-deformation model

The model developed by Gangi (1978, 1981) and Gangi and Carlson (1996) predicts the wave velocity of a cracked medium as a function of effective pressure. The model is based on the calculation of the fractional area of contact of the asperities between the shale platelets, which is a key physical quantity affecting the stiffness moduli of the rock. At low pressures, the mechanical properties of the rock are dominated by the behaviour of cracks and pores, in particular by the area of contact of the asperities on the surface of the platelets constituting the shale. As the cracks close, the asperities are compressed, more asperities come into contact, making the rock stiffer, the load is supported by the asperities and the area of contact increases.

The undrained P- and S-wave compliances of a porous cracked rock can be expressed as

$$\frac{1}{M} = \frac{\phi_L(P_c,\,P_a)}{(1 - P_p A'_f)M_a(P_a) + [1 - A_f(P_a)]K_f(P_p)} + \frac{1 - \phi_L(P_c,\,P_a)}{M_g(P_c)} = \frac{1}{\rho v_P^2} \tag{6}$$

and

$$\frac{1}{\mu} = \frac{\phi_L(P_c,\,P_a)}{(1 - P_p A'_f)\mu_a(P_a)} + \frac{1 - \phi_L(P_c,\,P_a)}{\mu_g(P_c)} = \frac{1}{\rho v_S^2} \tag{7}$$

(Gangi and Carlson 1996), where v_P and v_S are the wave velocities, ρ is the bulk density, P_c is the confining pressure, P_p is the pore pressure, K_f is the pore-fluid modulus, M_g is the P-wave modulus of the grains, ϕ_L is the linear porosity, μ_g is the shear modulus of the grains,

$$P_a = P_c - (1 - A_f)P_p = P_c - nP_p \tag{8}$$

is the effective pressure (or asperity pressure), A_f is the fractional area of contact of the asperities in the crack, n is the effective-stress coefficient, $A'_f = \mathrm{d}A_f/\mathrm{d}P_a$, and M_a and μ_a are the P- and S-wave moduli due to the asperities alone.

Equation (8) provides a physical explanation of the effective-stress coefficient. It is the fraction of crack which is not in contact. Note that Biot's effective-stress coefficient is $1 - K_m/K_g$, where K_m is the dry-rock bulk modulus and K_g is the bulk modulus of the grains (e.g. Carcione 2001). No contact between grains means that $K_m = 0$ (a suspension of grains in the fluid), which is consistent with $A_f = 0$.

The bulk density is given by

$$\rho = (1 - \phi)\rho_g(P_c) + \phi\rho_f(P_p), \tag{9}$$

where ρ_g is the grain density, ρ_f is the fluid density, and ϕ is the volume porosity given by equation (3).

The determination of the area of contact is based on the bed-of-nails model, which assumes rod-like asperities whose height distribution has a power-law (or fractal) behaviour (Gangi 1978, 1981; see Fig. 1). The crack width w is given by

$$\frac{w}{w_0} = 1 - \left(\frac{P_i + P_a}{P_1}\right)^m, \tag{10}$$

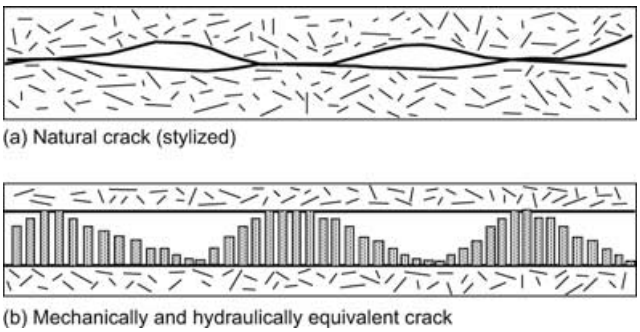

Figure 1 (a) A natural crack and (b) mechanically and hydraulically equivalent 'bed-of-nails' crack. The geometry of a real crack is approximated by a mechanically equivalent distribution of cylindrical rods of different length (after Gangi 1978, 1981). The random packing of spheres corresponding to the Hertz–Mindlin model is shown in (c), where the contact area between the grains depends on the differential pressure.

where P_i is the equivalent initial effective pressure, which gives the initial area of contact, P_1 is a constant approximately equal to the bulk modulus or Young's modulus of the rock material, m characterizes the power-law asperity-height distribution, and w_0 is the width when $P_a = -P_i$. That is, to obtain w_0, it is necessary to put the rock under tension (or have the pore pressure greater than the confining pressure) for a finite equivalent initial pressure. The tension is necessary to break the bonds of the asperities that do not have zero contact area when the effective pressure is zero.

The initial crack width w_0 is also the maximum possible length of any asperity. When pressure is applied to the rock, the walls of the crack move together and more rods come into contact, while those already in contact are compressed. Since the rods act as springs, the stiffness of the system increases with increasing pressure. The distribution of rod lengths can be approximated by a power-law distribution function, such that the crack width can be expressed in terms of the effective pressure as in equation (10). This equation corresponds to a non-through-going crack, where some asperities are in contact when no pressure is applied because of interlocking grains and/or cementation ($w = w_0$ when $P_a = -P_i$).

The fractional area of contact is given by

$$A_f = \frac{P_1}{mE}\left(\frac{P_i + P_a}{P_1}\right)^{1-m} \tag{11}$$

and

$$A_f' = \frac{dA_f}{dP_a} = \frac{1-m}{mE}\left(\frac{P_i + P_a}{P_1}\right)^{-m}, \tag{12}$$

where E is Young's modulus. These equations hold for $(P_i + P_a)/P_1 < 0.1$, which, in general, holds for effective pressures as large as 200 MPa, corresponding to normally pressured and over-pressured sediments to about 10 km depth.

Since $M_a = -w\,(dP_a/dw)$ and using equations (10) and (11), we obtain

$$M_a \approx \frac{P_1}{m}\left(\frac{P_i + P_a}{P_1}\right)^{1-m} = E\,A_f. \tag{13}$$

Similarly, μ_a has the form,

$$\mu_a \approx \mu_0\left(\frac{P_i + P_a}{P_1}\right)^{1-m}. \tag{14}$$

Because the fractional area of contact is a function of the effective pressure itself (see equations (8) and (11)), we use the following approximation of the effective-stress coefficient:

$$n \approx 1 - \frac{P_1}{mE}\left(\frac{P_i + P_d}{P_1}\right)^{1-m}, \tag{15}$$

where we have replaced the effective pressure P_a by the differential pressure $P_d = P_c - P_p$ in equation (11).

The linear porosity ϕ_L is given by

$$\phi_L = \frac{w}{L} = \phi_{L0}\left[1 - \left(\frac{P_i + P_a}{P_1}\right)^m\right], \tag{16}$$

where L is the length of the rock and ϕ_{L0} is the porosity at $P_a = -P_i$.

Experiments on samples at zero pore pressure and varying confining pressure allow the determination of E, P_i, P_1, m and ϕ_{L0}. The parameters E and ϕ_{L0} have to be measured directly (or estimated), while P_i, P_1 and m are fitting parameters when a data set is fitted with the theoretical equations for mechanical and/or transport-property variations with pressure (and/or temperature) (see e.g. Carlson and Gangi 1985; Gangi and Carlson 1996).

Let us assume two different states of the rock, with lengths L and L', porosities ϕ_L and ϕ'_L, and P-wave velocities v_P and v'_P. Then, the following relationship between length and porosity holds:

$$\frac{L}{L'} = \frac{1-\phi'_L}{1-\phi_L}, \tag{17}$$

and

$$\frac{\Delta L}{L} = \frac{\phi'_L - \phi_L}{1-\phi'_L} \simeq \frac{\Delta\phi_L}{1-\phi_L}, \tag{18}$$

where $\Delta L = L' - L$ and $\Delta\,\phi_L = \phi'_L - \phi_L$.

On the other hand,

$$\frac{\Delta v_P}{v_P} = \sqrt{\frac{M'}{M}\frac{\rho}{\rho'}} - 1, \tag{19}$$

where $\Delta v_P = v'_P - v_P$.

The parameter α (equation (2)) is given by

$$\alpha = \frac{\Delta v_P}{v_P}\left(\frac{\Delta L}{L}\right)^{-1}, \tag{20}$$

which, using equations (18) and (19), becomes

$$\alpha = \frac{1-\phi'_L}{\phi'_L - \phi_L}\left(\sqrt{\frac{v'_P}{v_P}} - 1\right) = \frac{1-\phi'_L}{\phi'_L - \phi_L}\left(\sqrt{\frac{M'}{M}\frac{\rho}{\rho'}} - 1\right). \tag{21}$$

The preceding equations hold for isotropic deformations (expansion or compaction). For uniaxial deformations the linear porosity has to be replaced by the volume porosity. The demonstration of equation (18) for the two cases (see Appendix A) is shown in two dimensions, due to its simplicity, but the equations hold for the three-dimensional case as well.

The Hertz–Mindlin model

In the absence of calibration data, the classical model to obtain the dry-rock moduli as a function of the effective (differential) pressure is the Hertz–Mindlin contact theory, which considers spherical grains (Fig. 1c). The stresses are calculated in terms of the strains by considering the random packing of spheres as an effective medium that exerts a mean-field force (as given by contact Hertzian theory) on a single representative grain. This calculation gives the effective stiffness moduli.

We modify the Hertz–Mindlin model by replacing the differential pressure, P_d, by the augmented differential pressure, $P_d + P_i$, following Gangi (1978, 1981). Then, the dry-rock bulk and shear moduli at the critical porosity are given by

$$K_{mc} = \left[\frac{C^2(1-\phi_c)^2\mu_g^2(P_d + P_i)}{18\pi^2(1-\nu_g)^2}\right]^{1/3} \tag{22}$$

and

$$\mu_{mc} = \frac{3(5-4\nu_g)}{5(2-\nu_g)}K_{mc}, \tag{23}$$

where μ_g is the shear modulus of the grains, ν_g is Poisson's ratio of the grains, ϕ_c is the critical porosity and C is the average number of contacts per spherical grain. The critical porosity is the porosity above which the moduli are very small, i.e. the rock becomes a liquid suspension ($\phi_c = 0.36$ for a random dense pack of identical spherical grains). An approximate equation for C, based on Murphy's (1982) data, is $C = 3.05/\phi_c$.

Walton (1987) and Mavko, Mukerji and Dvorkin (1998) obtained a model for infinitely rough spheres and ideally smooth spheres. The first is identical to the Hertz–Mindlin model described above, and the second has the same bulk modulus as the Hertz–Mindlin model but a different shear modulus, namely,

$$\mu_{mc} = \frac{3}{5}K_{mc} \tag{24}$$

(note that this relationship corresponds to a Poisson's solid).

To obtain the dry-rock moduli, we may use different models depending on whether the rock is consolidated or unconsolidated. In the first case, we use a Hill average, i.e. an arithmetic average of the Voigt and Wood moduli:

$$K_m = \frac{1}{2}(K_V + K_W) \quad \text{and} \quad \mu_m = \frac{1}{2}(\mu_V + \mu_W), \tag{25}$$

where

$$K_V = (1-\phi/\phi_c)K_g + (\phi/\phi_c)K_{mc}, \qquad \frac{1}{K_W} = \frac{1-\phi/\phi_c}{K_g} + \frac{\phi/\phi_c}{K_{mc}}, \tag{26}$$

$$\mu_V = (1-\phi/\phi_c)\mu_g + (\phi/\phi_c)\mu_{mc} \quad \text{and}$$
$$\frac{1}{\mu_W} = \frac{1-\phi/\phi_c}{\mu_g} + \frac{\phi/\phi_c}{\mu_{mc}}, \tag{27}$$

where K_g is the bulk modulus of the grains. Note that ϕ is the volume porosity, which is related to the linear porosity ϕ_L by equation (3).

For unconsolidated rocks, we use the modified Hashin–Shtrikman lower bound introduced by Dvorkin and Nur (1996). In this case,

$$K_m = \Lambda(\mu_{mc}) \tag{28}$$

and

$$\mu_m = \Gamma[\xi(K_{mc}, \mu_{mc})], \tag{29}$$

where

$$\Lambda(\mu_\pm) = \left\langle \frac{1}{K + \frac{4}{3}\mu_\pm} \right\rangle^{-1} - \frac{4}{3}\mu_\pm, \tag{30}$$

$$\Gamma(\xi) = \left\langle \frac{1}{\mu + \xi} \right\rangle^{-1} - \xi, \tag{31}$$

$$\xi(K_\pm, \mu_\pm) = \frac{\mu_\pm}{6}\left(\frac{9K_\pm + 8\mu_\pm}{K_\pm + 2\mu_\pm}\right) \tag{32}$$

(see e.g. Mavko *et al.* 1998), and the subscripts + and − denote the maximum and minimum moduli of the single constituents. The brackets $\langle\cdot\rangle$ indicate an average over the constituents weighted by their volume fractions. As above, the composite moduli are those of the mineral grains, defined by K_g and μ_g, when $\phi = 0$.

The bulk modulus of the wet rock is given by the Gassmann modulus,

$$K = K_m + \gamma^2 M, \tag{33}$$

where

$$\gamma = 1 - \frac{K_m}{K_g} \quad \text{and} \quad M = \left(\frac{\gamma - \phi}{K_g} + \frac{\phi}{K_f}\right)^{-1} \tag{34}$$

(e.g. Carcione 2001, p. 225). The shear modulus of the wet rock is simply the modulus of the dry rock, $\mu = \mu_m$. The P- and S-wave velocities are then

$$v_P = \sqrt{\frac{K + 4\mu/3}{\rho}} \quad \text{and} \quad v_S = \sqrt{\frac{\mu}{\rho}}, \tag{35}$$

where ρ is the bulk density, given by

$$\rho = (1-\phi)\rho_g + \phi\rho_f. \tag{36}$$

The porosity variation with differential pressure of the Hertzian rock is given by

$$\phi = \frac{\phi_0 A}{1 + \phi_0(A-1)}, \text{ with}$$
$$A = \left[1 - \frac{1}{1-\sqrt{2/3}}\left(\frac{P_d + P_i}{P_0}\right)^{2/3}\right]^3 \tag{37}$$

(Gangi 1981), where ϕ_0 is the porosity of the pack of spheres at 'zero loading' (i.e. for $P_d = -P_i$ or $A = 1$), $P_0 = 4E/[3\pi(1-\nu_g^2)]$, $E = 2\mu_g(1+\nu_g)$, and ν_g is Poisson's ratio of the grains. The augmenting pressure, P_i, or equivalent initial pressure, for a low-porosity rock can be determined using equations (37) with $P_d = 0$:

$$\frac{P_i}{P_0} = \left(1 - \sqrt{2/3}\right)^{3/2}\left\{1 - \left[\frac{\phi_i(1-\phi_0)}{\phi_0(1-\phi_i)}\right]^{1/3}\right\}^{3/2} \tag{38}$$

where ϕ_i is the 'cemented'-rock's porosity at zero differential pressure.

As in the previous section, we define the parameter α as

$$\alpha = \frac{1-\phi'_L}{\phi'_L - \phi_L}\left(\sqrt{\frac{v'_P}{v_P}} - 1\right), \tag{39}$$

where

$$\phi_L = 1 - (1-\phi)^{1/3} \tag{40}$$

(see equation (3)), and the prime denotes a different pressure regime.

EXAMPLES

We model changes in the overburden rock (shale) by varying the confining pressure P_c while keeping the pore pressure P_p constant. We consider a water-saturated layer at a confining pressure of 70 MPa and a pore pressure of 30 MPa, which corresponds to a layer at approximately 2.5 to 3 km depth. We vary P_c from 70 MPa to 35 MPa and compute the velocity of the rock, the value of α and the traveltime changes.

The parameters for the asperity-deformation model are: $m = 0.2$, $P_1 = 23$ GPa, $E = 25$ GPa, $\phi_0 = 0.1$ (volume porosity), $M_g = 25$ GPa, $\rho_g = 2650$ kg/m^3, $K_f = 2.25$ GPa and $\rho_f = 1030$ kg/m^3. Figure 2 shows the P-wave velocity as a function of porosity (a); and α (b) and (e), the P-wave velocity variations (c), and the traveltime variations (d) and (f) as a function of thickness changes. Curves (a), (b), (c) and (d) correspond to an isotropic ('hydrostatic') deformation, while curves (e) and (f) correspond to a uniaxial deformation. The curves correspond to initial effective pressures $P_i = 2.5$ MPa

(solid line), 5 MPa (dotted line), 10 MPa (dashed line) and 20 MPa (dashed-dotted line). The wave-velocity curves in (a) are shifted for a better display (the correct location is given by the solid line). For increasing initial effective pressure (initial area of contact), the velocity increases and the porosity decreases, while the absolute value of α increases. As the differential pressure decreases, α decreases in absolute value. For example, consider Fig. 2(d): if $L = 1000$ m, $T = 1.5$ s and $\Delta L/L = 0.2\%$, we have $\Delta T/T = 1.2\%$, and therefore $\Delta L =$ 2 m and $\Delta T = 18$ ms. The values of α for uniaxial deformations are smaller (in absolute value) than the values for isotropic deformations, much more in agreement with the regressions studied by Hatchell and Bourne (2005a,b). Moreover, the length and traveltime variations are almost three times larger. However, note that the uniaxial stress condition requires the use of anisotropic constitutive relationships to be more accurate.

Next, we consider the Hertz–Mindlin model for consolidated (shale) rocks, with $K_g = 20$ GPa, $\mu_g = 10$ GPa, $\rho_g = 2600$ kg/m^3, $K_f = 2.25$ GPa, $\rho_f = 1030$ kg/m^3, $\phi_c = 0.39$ and $\phi_0 = 0.33$. Figure 3 shows the P-wave velocity as a function of porosity (a); and α (b), the P-wave velocity variations (c), and the traveltime variations (d) as a function of thickness changes. The curves correspond to $P_i = 100$ MPa (solid line), 150 MPa (dotted line), 200 MPa (dashed line) and 250 MPa (dashed-dotted line). The behaviour of these curves is qualitatively similar to those of the asperity-deformation model. The

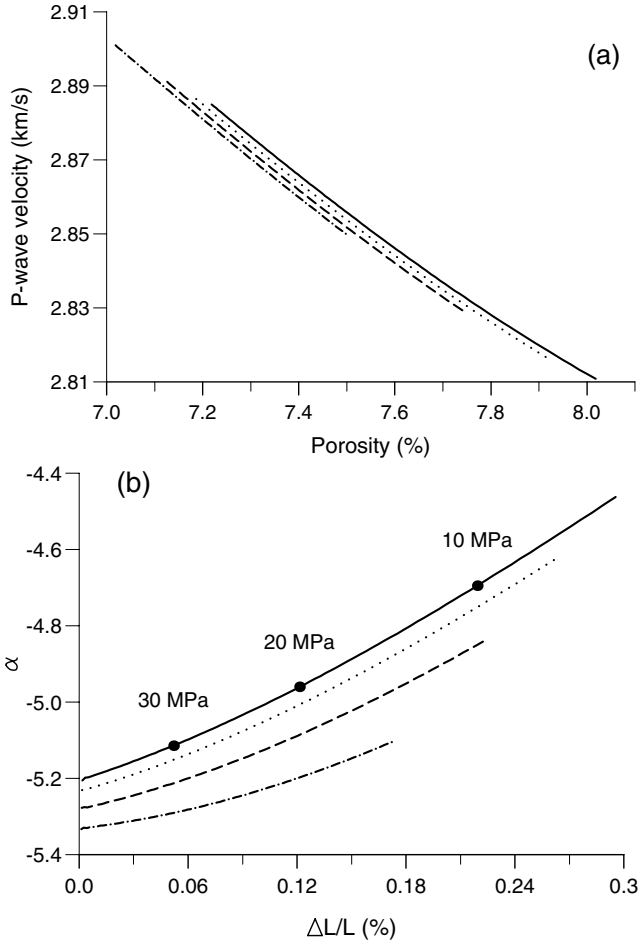

Figure 2 Asperity-deformation model for shale, where $P_i = 2.5$ MPa (solid line), 5 MPa (dotted line), 10 MPa (dashed line) and 20 MPa (dashed-dotted line); (a) P-wave velocity as a function of porosity; (b), (e) α, (c) P-wave velocity variations, and (d), (f) traveltime variations as a function of thickness change. Curves (a), (b), (c) and (d) correspond to an isotropic ('hydrostatic') deformation, while curves (e) and (f) correspond to an uniaxial deformation. The wave-velocity curves in (a) are shifted for a better display (the correct location is given by the solid line). The value of the differential pressure is indicated by dots in one of the curves; $P_d = 40$ MPa and 5 MPa at the left-hand and right-hand ends, respectively, of all the curves.

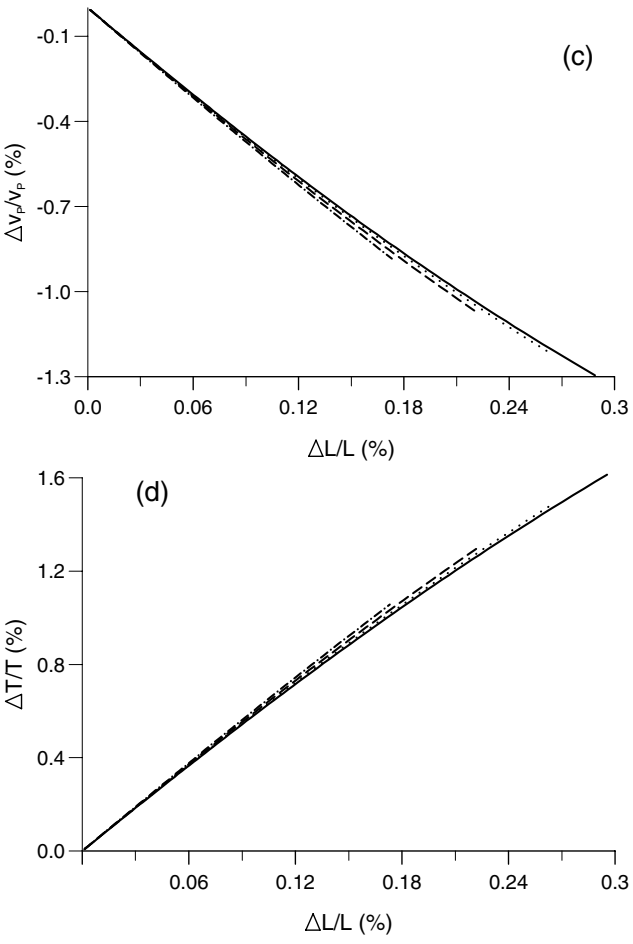

Figure 2 Continued.

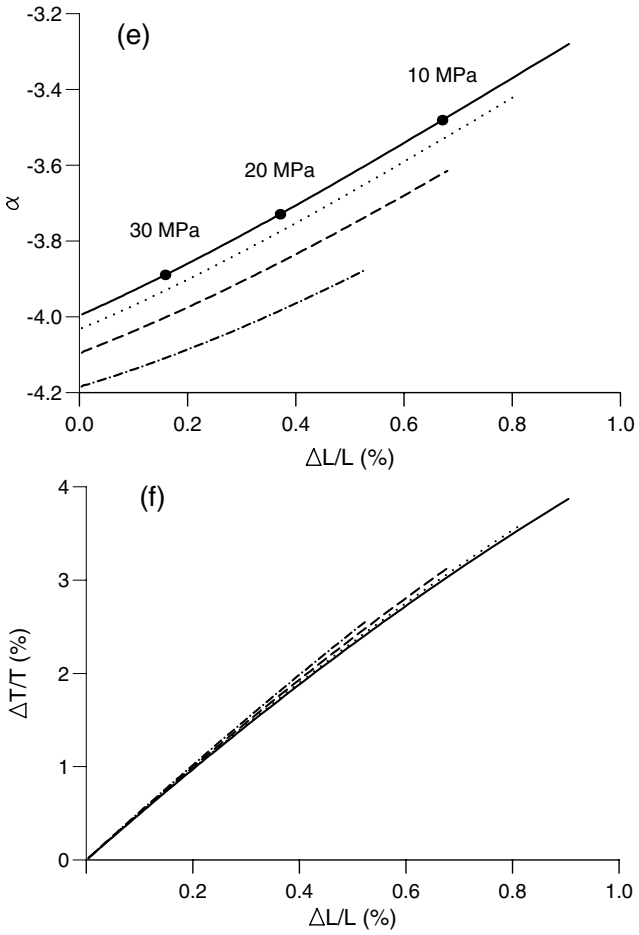

Figure 2 Continued.

Hertz–Mindlin model requires higher initial effective pressures to model the initial shale porosities, and the thickness changes are larger. For example, if $L = 1000$ m, $T = 1.5$ s and $\Delta L/L = 1\%$, we have $\Delta T/T = 3\%$, $\Delta L = 10$ m and $\Delta T = 45$ ms.

The results of the Hertz–Mindlin model applied to a reservoir rock (sandstones) are shown in Fig. 4, where $K_g = 40$ GPa, $\mu_g = 35$ GPa, $P_i = 10$ MPa, and the other properties are the same as those in the previous example. In this case, the absolute values of α are larger compared with those of shale, and they increase as a function of the thickness change. The velocity and traveltime variations are larger than those of shale for the same thickness changes. The dilation factor can be highly affected for reservoirs rocks, compared with shales, due to pressure depletion causing gas coming out of solution, since this process has a large effect on seismic velocities (Carcione and Gangi 2000).

Let us consider the following linear empirical law relating velocity and porosity: v [km/s] $= 5.81 - 9.42\ \phi - 2.21\ V_{cl}$

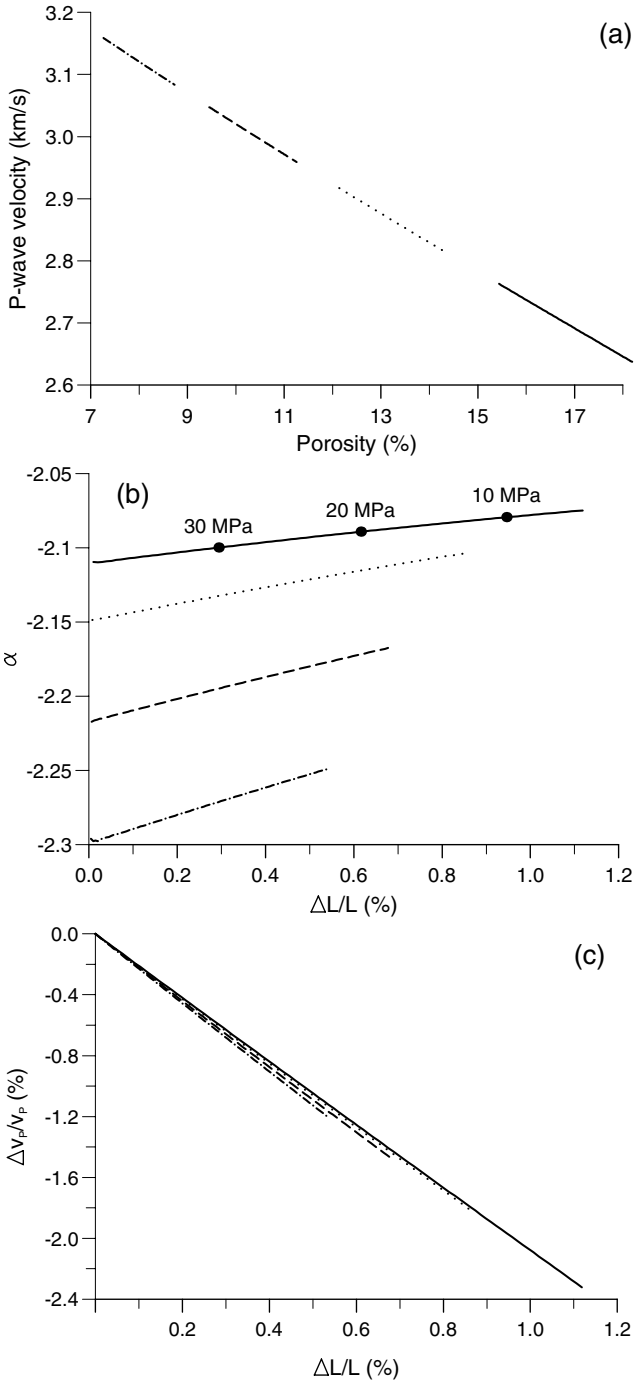

Figure 3 Hertz–Mindlin model for shale, where $P_i = 100$ MPa (solid line), 150 MPa (dotted line), 200 MPa (dashed line) and 250 MPa (dashed-dotted line); (a) P-wave velocity as a function of porosity; (b) α, (c) P-wave velocity variations, and (d) traveltime variations as a function of thickness change. The value of the differential pressure is indicated by dots in one of the curves; $P_d = 40$ MPa and 5 MPa at the left-hand and right-hand ends, respectively, of all the curves.

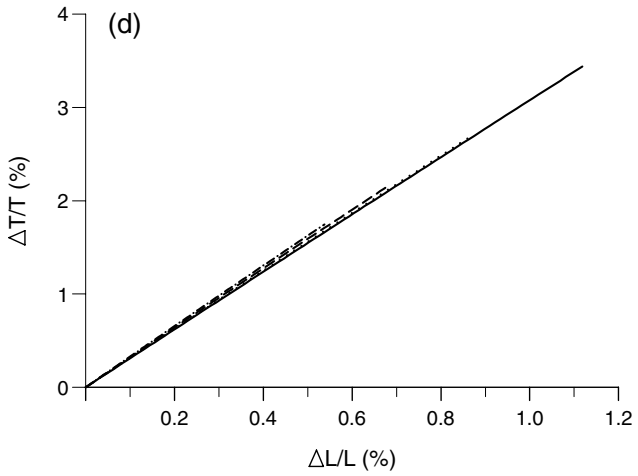

Figure 3 Continued.

(Castagna, Batzle and Eastwood 1985), where the clay volume fraction is $V_{cl} = 0.95$. The value of α (for isotropic deformations) is given by $9.42(\phi - 3)/v \approx -9.2$, i.e. nearly constant (for uniaxial deformations the corresponding value is -3.1) (see Introduction). In fact, this α is not comparable with those of Figs 2(b) and 3(b), because they correspond to the same rock that is subject to variation of the effective pressure, while the value $\alpha = -9.2$ corresponds to different rocks at the same effective pressure.

Observing the curves in Figs 2, 3 and 4, we may infer that the trends are approximately linear, especially for the asperity-deformation model. In particular $\alpha = A + B\,x$, where $x = \Delta L/L$ and A and B are constants, with $A < 0$. Hence, the velocity variations are given by $A\,x + B\,x^2$ (see equation (2)), and the thickness changes, in terms of the traveltime variations, can be obtained by solving the following second-order equation: $B\,x^2 - (1 - A)\,x + \Delta T/T = 0$ (see equation (5)). However, the quadratic term is not significant, because the relationship between $\Delta T/T$ and $\Delta L/L$ is approximately linear, as can be seen in Figs 2(d) and 3(d).

The last example considers real logs (see Fig. 5a). We distinguish two cases:

1 the variations in the log velocities are due to the grain moduli (Fig. 5b);
2 the variations are due to changes in augmented differential pressure (Fig. 8).

Case 1 The augmented differential pressure is held constant at $P_d + P_i = 20$ MPa, the bulk density is ρ = 2210 kg/m^3 and the porosity is ϕ = 0.1, with $\phi_c = 0.41$. The layers constituting

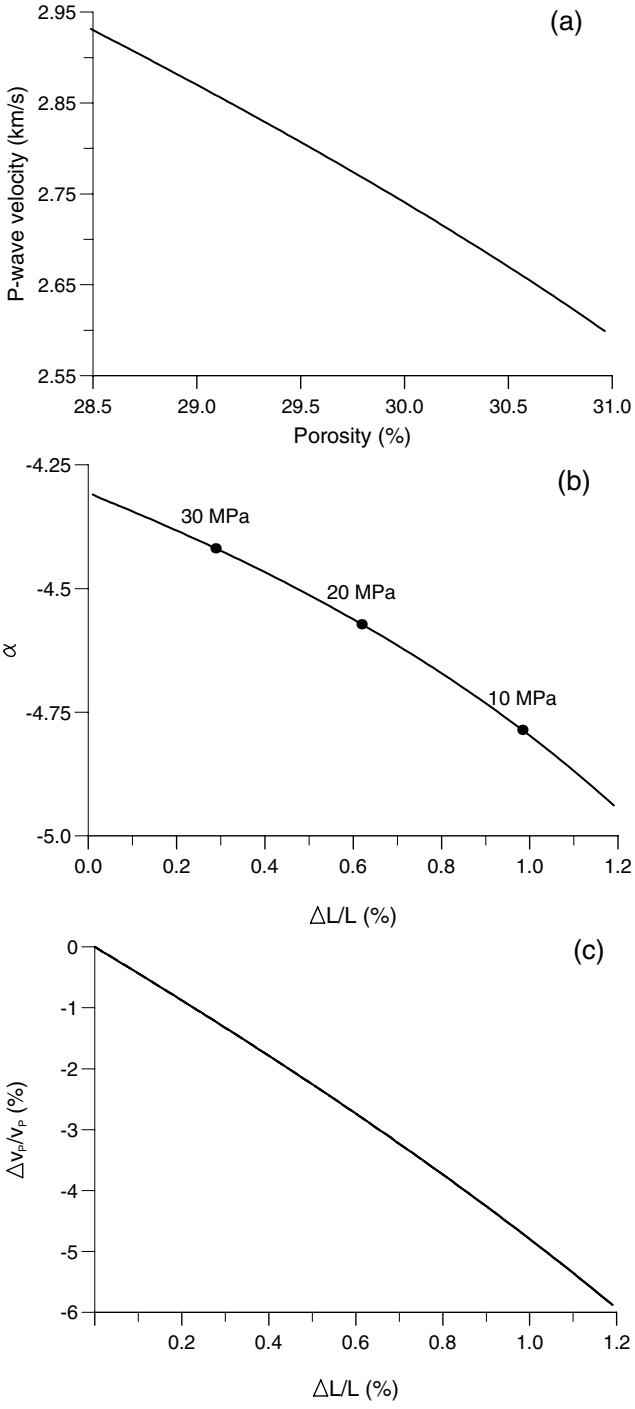

Figure 4 Hertz–Mindlin model for sandstone, where $P_i = 10$ MPa; (a) P-wave velocity as a function of porosity; (b) α, (c) P-wave velocity variations, and (d) traveltime variations as a function of thickness change. The value of the differential pressure is indicated by dots in one of the curves; p_d = 40 MPa and 5 MPa at the left-hand and right-hand ends, respectively, of all the curves.

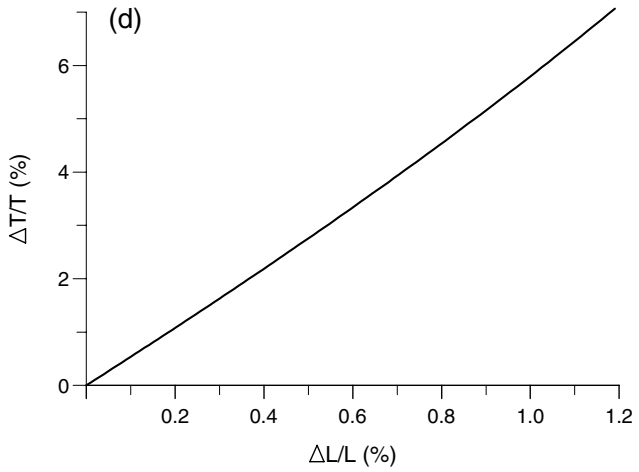

Figure 4 Continued.

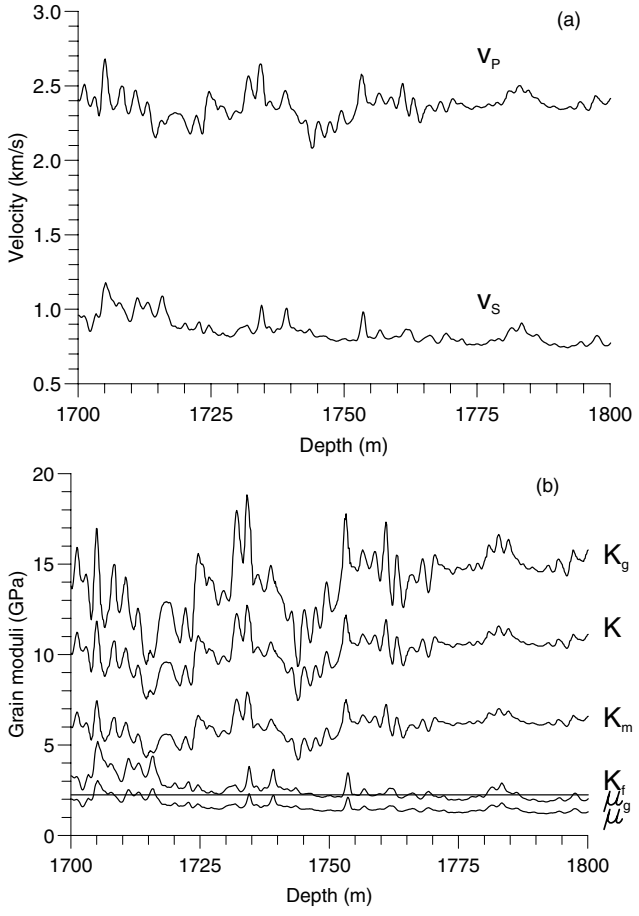

Figure 5 Well logs of P- and S-wave velocities (a), and different moduli (b) as a function of depth for a shale sequence in the North Sea. The Hertz–Mindlin model was used to obtain the moduli from the velocity logs. The augmented differential pressure is held constant at $P_d + P_i = 20$ MPa.

the sequence are filled with brine, with $K_f = 2.25$ GPa and $\rho_f = 1030$ kg/m^3. All the above quantities are assumed to be constant along the sequence. The Hertz–Mindlin model is used to model the seismic properties (elastic moduli and parameter α) of the sequence, assuming that the variations observed in the velocity logs are due to changes in the grain elastic moduli only. The calculation proceeds as follows:

1 The grain density is obtained from the composite density (equation (9)).
2 The second equation (35) is used to obtain the dry-rock shear modulus $\mu_m = \mu$.
3 Gassmann's modulus is obtained from the first equation (35).
4 Because Poisson's ratio of the grain and the dry-rock moduli is

$$\nu_g = \frac{3K_g - 2\mu_g}{2(3K_g + \mu_g)}$$

and, from equations (33)–(35),

$$K_m = \frac{(\phi K_g/K_f + 1 - \phi)K - K_g}{\phi K_g/K_f + K/K_g - 1 - \phi}$$

(e.g. Carcione 2001, p. 225) then K_g and μ_g can be obtained from equations (25)–(27), using equations (22) and (23).
5 An α log can be obtained from equations (39) and (40) by varying the differential pressure, using the grain moduli computed previously, and assuming $P_i = 20$ MPa.

Two α logs are shown in Fig. 6, where $\phi_0 = 0.11$, and the initial and final differential pressures are 1 and 11 MPa (lower

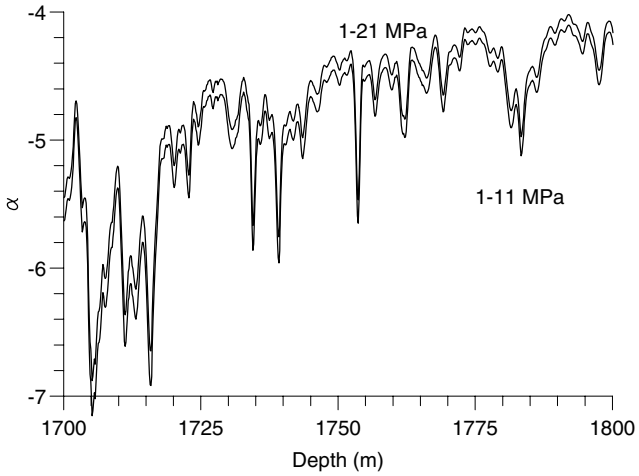

Figure 6 Parameter α as a function of depth corresponding to the layer sequence shown in Fig. 5. The initial and final differential pressures are 1 and 11 MPa (lower log), and 1 and 21 MPa (upper log), respectively.

log), and 1 and 21 MPa (upper log), respectively. As can be seen, α decreases (in absolute value) with depth and increasing differential pressure. These logs give an estimate of realistic values of α for a shale sequence.

Case 2 In Case 1, we assumed that the augmented differential pressure remains constant throughout the vertical profile, while here we compute it under the assumption that Poisson's ratio of the grain is the same as that of the saturated rock. This assumption appears to be reasonably justified, as these ratios are indeed only slightly different in Case 1 (see Fig. 7). The resulting vertical profile of augmented differential pressure is shown in Fig. 8. In addition, Fig. 9 shows a comparison between the elastic moduli estimated in Case 1 (continuous lines) and in Case 2 (dashed lines): we note that the estimate of the bulk modulus is very robust, while the difference between the two estimates of the shear modulus is noticeable.

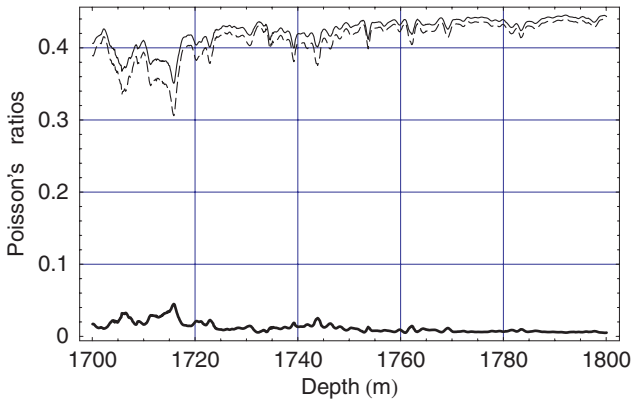

Figure 7 Poisson's ratios of saturated rock (thin continuous line) and of grain (dashed line) considered in Case 1, plotted versus depth (in m). The difference between the two ratios (thick continuous line) is also shown.

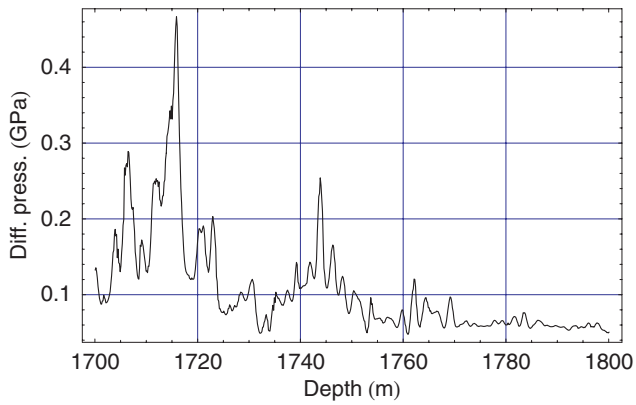

Figure 8 Augmented differential pressure (in GPa) estimated in Case 2, plotted versus depth (in m).

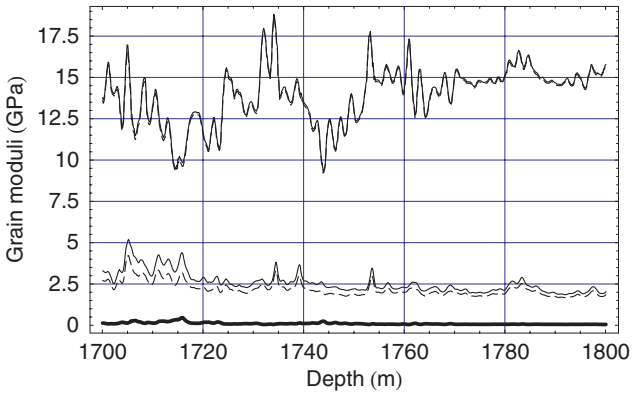

Figure 9 Comparison of grain moduli (in GPa) estimated in Case 1 (thin continuous line) and in Case 2 (dashed line), plotted versus depth (in m). The two upper lines (almost coincident) represent bulk moduli, while the two central lines represent shear moduli. The augmented differential pressure (in GPa) estimated in Case 2 (see Fig. 8) is also shown (thick continuous line).

CONCLUSIONS

We have derived expressions for the dilation factor representing the relative changes in seismic velocity with respect to the fractional changes in layer thickness. The factor has been derived for two petro-elastic models, describing a wide range of rock types. The dilation factor is negative, and its absolute value generally decreases for shale and increases for sandstone when the layer thickness increases and the effective pressure decreases. The thickness changes in the reservoir or overburden rocks can be obtained by solving a second-order polynomial equation in terms of the observed time-lapse traveltime variations. Nevertheless, for practical purposes, the dilation factor can be assumed to be constant; i.e. fractional changes in thickness and velocity are linearly related. However, before reaching a definite conclusion, other effects in reservoir rocks need to be investigated, such as the asymmetry of the dilation factor with respect to expansion and compaction, and the effects of gas coming out of solution after pressure depletion, since this process affects the pore-fluid properties and therefore the seismic velocities.

Knowledge of the dilation factor is essential for distinguishing between velocity and layer changes when processing 4D time-lapse data in order to determine reservoir and overburden compaction/stretching and surface subsidence due to the production of hydrocarbons. Most 4D techniques aimed at determining the dilation factor are associated with significant uncertainties. In this context, we believe that the equations derived here might be used to constrain 4D inversion for simultaneous estimation of thickness and velocity changes.

ACKNOWLEDGEMENTS

J.M.C. and M.L. acknowledge financial support from the Norwegian Research Council through the Rock Seismic (ROSE) project at NTNU. The authors thank two anonymous reviewers for useful comments.

REFERENCES

Carcione J.M., 2001. *Wave Fields in Real Media: Wave Propagation in Anisotropic, Anelastic and Porous Media. Handbook of Geophysical Exploration*, vol. 31. Pergamon Press Inc.

Carcione J.M. and Gangi A., 2000. Gas generation and overpressure: effects on seismic attributes. *Geophysics* **65**, 1769–1779.

Carlson R.L. and Gangi A.F., 1985. Effect of cracks on the pressure dependence of P-wave velocities in crystalline rocks. *Journal of Geophysical Research* **90**, 8675–8684.

Castagna J.P., Batzle, M.L. and Eastwood R.L., 1985. Relationships between compressional-wave and shear-wave velocities in clastic silicate rocks. *Geophysics* **50**, 571–581.

Dvorkin J. and Nur A., 1996. Elasticity of high-porosity sandstones: Theory for two North Sea data sets. *Geophysics* **61**, 1363–1370.

Gangi A.F., 1978. Variation of whole and fractured porous rock permeability with confining pressure. *International Journal of Rock Mechanics and Mining Sciences* **15**, 249–257.

Gangi A.F., 1981. The variation of mechanical and transport properties of cracked rocks with pressure. *Proceedings of 22nd U.S. Symposium on Rock Mechanics*, pp. 85–89.

Gangi A.F. and Carlson R.L., 1996. An asperity-deformation model for effective pressure. *Tectonophysics* **256**, 241–251.

Guilbot J. and Smith B., 2002. 4-D constrained depth conversion for reservoir compaction estimation: Application to Ekofisk Field. *The Leading Edge* **21**, 302–308.

Hatchell P.J. and Bourne S.J. 2005a. Rocks under strain: Strain-induced time-lapse time shifts are observed for depleting reservoirs. *The Leading Edge* **24**, 1222–1225.

Hatchell P.J. and Bourne S.J. 2005b. Measuring reservoir compaction using time-lapse timeshifts. 75th SEG Meeting, Houston, USA, Expanded Abstracts, 2500–2503.

Hatchell P.J., Kawar, R.S. and Savitski A.A., 2005. Integrating 4D seismic, geomechanics and reservoir simulation in the Valhall oil field. 67th EAGE Conference, Madrid, Spain, Extended Abstracts, C012.

Hertz H., 1895. *Gesammelte Werke, Band I, Schriften Vermischten Inhalts*, Leipzig.

Mavko G., Mukerji, T. and Dvorkin J., 1998. *The Rock Physics Handbook: Tools for Seismic Analysis in Porous Media*. Cambridge University Press.

Mindlin R.D., 1949. Compliance of elastic bodies in contact. *Journal of Applied Mechanics* **16**, 259–268.

Murphy W.F., 1982. *Effects of microstructure and pore fluids on the acoustic properties of granular sedimentary materials*. PhD thesis, Stanford University.

Røste T., Stovas, A. and Landrø, M., 2006. Estimation of layer thickness and velocity changes using 4D prestack seismic data. *Geophysics* **71(6)**, S219–S234.

Walton K., 1987. The effective elastic moduli of a random packing of spheres. *Journal of the Mechanics and Physics of Solids* **35**, 213–226.

APPENDIX A

The difference between isotropic and uniaxial expansions

Equation (18) holds for isotropic deformations. This equation is demonstrated here, and the equivalent equation for uniaxial deformations is obtained.

For simplicity, we consider the 2D case. Let us assume a square sample of rock of length L, having two orthogonal cracks of width w. After an isotropic expansion by an amount ΔL, the length of the sample is $L + \Delta L$ and the crack width is $w + \Delta L$. We obtain

$$\begin{aligned} &L^2\phi = 2wL - w^2, \\ &(L+\Delta L)^2\phi' = 2(w+\Delta L)(L+\Delta L) - (w+\Delta L)^2. \end{aligned} \tag{A1}$$

Since the linear porosity is $\phi_L = w/L$, we have $\phi = 2\,\phi_L - \phi_L^2$. Subtracting the two equations (A1), we obtain

$$\frac{\Delta\phi}{1-\phi'} = \frac{2\Delta L}{L} + \left(\frac{\Delta L}{L}\right)^2, \tag{A2}$$

where $\Delta\,\phi = \phi' - \phi$. Neglecting the second term on the right-hand side and assuming $\phi \approx 2\,\phi_L$, it can be shown that equation (A2) is a good approximation to equation (18) for $\phi \ll 1$.

On the other hand, for an uniaxial expansion, the second equation (A1) has to be replaced by

$$L(L+\Delta L)\phi' = 2wL + L\Delta L - w^2. \tag{A3}$$

Subtracting this equation from the first equation (A1) gives

$$\frac{\Delta L}{L} = \frac{\Delta\phi}{1-\phi'} \simeq \frac{\Delta\phi}{1-\phi} \tag{A4}$$

(Guilbot and Smith 2002).

APPENDIX B

List of symbols

A_f	fractional area of contact
α	dilation factor
C	average number of contacts per spherical grains
ΔL	layer-thickness variation
ΔT	traveltime variation
Δv	P-wave seismic-velocity variation
E	grain Young modulus

ϕ	volume porosity
$\phi_{\rm c}$	critical porosity
$\phi_{\rm i}$	porosity at zero differential pressure
ϕ_L	linear porosity
$\phi_{\rm L0}$	linear porosity at $P_{\rm a} = -P_{\rm i}$
ϕ_0	porosity at $P_{\rm a} = -P_{\rm i}$
K	Gassmann modulus
$K_{\rm f}$	fluid modulus
$K_{\rm g}$	grain bulk modulus
$K_{\rm m}$	dry-rock (matrix) bulk modulus
$K_{\rm mc}$	dry-rock bulk modulus at the critical porosity
$K_{\rm V}$	Voigt bulk modulus
$K_{\rm W}$	Wood bulk modulus
L	layer thickness
m	power-law asperity height exponent
M	wet-rock P-wave modulus
$M_{\rm a}$	dry-rock P-wave modulus
$M_{\rm g}$	grain P-wave modulus
μ	wet-rock S-wave modulus
μ_a	dry-rock shear modulus
μ_g	grain shear modulus
μ_{mc}	dry-rock shear modulus at the critical porosity
n	effective-stress coefficient
$\nu_{\rm g}$	Poisson ratio of the grains
$P_{\rm a}$	asperity (effective) pressure
$P_{\rm c}$	confining pressure
$P_{\rm d}$	differential pressure
$P_{\rm i}$	initial effective pressure
$P_{\rm p}$	pore pressure
P_0	$4\,E/[3\,\pi(1-\nu_g^2)]$
P_1	fitting parameter
ρ	bulk density
$\rho_{\rm f}$	fluid density
$\rho_{\rm g}$	grain density
T	traveltime
v	P-wave seismic velocity
$v_{\rm P}$	P-wave seismic velocity
$v_{\rm S}$	S-wave seismic velocity
w	crack width
w_0	crack width at $P_{\rm a} = -P_{\rm i}$